

1 **Validating response of AC microgrid to line-to-line short circuit in islanded mode using**
2 **dynamic analysis**

3

4

5 **Abstract**

6 This paper is presented in an attempt to validate the dynamic response of a microgrid to line-to-
7 line short circuit. The microgrid components include two identical Wind Turbine Generators
8 (WTGs) tied to a 100MVA, 13.8kV utility via a Point of Common Coupling (PCC). The utility-
9 microgrid testbed is modeled in SIMPOWERSystems® using two Doubly-Fed Induction
10 Generators (DFIGs) in the microgrid side. While in islanded operating mode, line-to-line short
11 circuit fault is applied at 6.0s and withdrawn at 8.0s, obtaining a 50.0s dynamic response of the
12 system for different fault locations, under voltage and reactive power control regimes of the wind
13 turbine controller. For measurement purpose, the absolute value of the stator complex voltage is
14 transformed to α, β, γ reference frame. Bidirectional power flow between the two feeders is
15 established in the study. The study also confirms that the microgrid composed of DFIGs offer
16 reactive power management capability, particularly by presenting superior performance when
17 stressed under Q control regime than under V control regime. Finally, the response of the testbed
18 to line-to-line short circuit has been validated and shown to be consistent with established short
19 circuit theory.

20

21 **Keywords:** Microgrid, Dynamic, DFIG, Microsource, Fault

22 **Abbreviations:** MS1 = Microsource 1, MS2 = Microsource 2, Feeder-a = Feeder connected to
23 microsource 1.

24

25 **1. Introduction**

26 The design and operation of power utility seek to generate, transmit and distribute electric power
27 in sufficiently large quantity and on uninterrupted basis to meet the contemporary and projected
28 future demands of the consumers in a load center. In order to achieve this goal, the system must
29 remain in operation continuously without long downtimes. Practically, achieving this goal
30 requires use of protective devices [1-4]. Protective devices function to achieve the following:

- 31 1. Minimize damage and repair costs whenever fault is sensed.
- 32 2. Safeguard the system to supply power continuously.
- 33 3. Consumer and personnel safety [5-9].

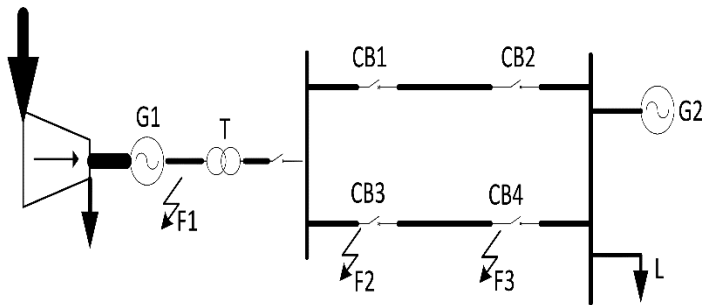
34 In order to meet above requirements, short circuit analyses are normally performed on the
35 system. The analysis will typically aim to determine the short-circuit rating of the equipment to
36 be purchased, installed and commissioned. Also, equipment manufacturers use the ratings
37 specified by their customers to ensure that their equipment are designed to satisfy client's safety
38 and operational specifications under certain conditions for specified duration [10-13]. As the
39 parameters of a power system and fault envelopes vary with time [14-16], short circuit analysis
40 which depicts the system dynamics is useful in order to achieve the utility operational goals -
41 ensuring high quality, continuous and safe delivery of power to consumers [17-20].

42 In this work, the authors present a utility-microgrid testbed for a research which aims at
43 proposing a new microgrid protection. Since the protection to be developed would be based on
44 measurement of three phase power, the nominal three phase active and reactive power is used and
45 presented in this paper. Thus, this paper presents an attempt to validate the response of the

46 modeled testbed to line-to-line short circuit. This is because the validity of the anticipated
 47 protection depends on the validity of the testbed's response to short circuit.

48 2. Short circuit in a power system

49 Consider a 3-phase to earth fault at point F2 as shown in fig. 1.



50

51 **Fig. 1.** Typical power system with short circuit points F1, F2 and F3

52 In an electric power generator, fault current is often initially around 8 times the full-load current. It
 53 attenuates rapidly to around 5 times full-load current before attenuating less rapidly to less than full-load
 54 current value. In the direct axis, this results in three stages of fault current envelop named sub-transient
 55 (x_d''), transient (x_d') and steady-state (x_d) respectively.

56 Fault F2 is therefore seen as a modified generator fault which incorporates the effect of
 57 transformer T. The transformer reactance, x_T , is added to the reactances x_d'' , x_d' and x_d as
 58 given in (1), (2) and (3) [4, 6, 7, 20].

59
$$x_d'' = X_d'' + X_T \quad (1)$$

60
$$x_d' = X_d' + X_T \quad (2)$$

61
$$x_d = X_d + X_T \quad (3)$$

62 The amplitude of the ac fault current in the sub-transient state, i_m'' , transient state, i_m' , and steady
 63 state, i_m^∞ , is presented in (4), (5) and (6), respectively.

$$64 \quad i_m'' = \frac{E_{fm}}{x_d''} \quad (4)$$

$$65 \quad i_m' = \frac{E_{fm}}{x_d'} \quad (5)$$

$$66 \quad i_m^\infty = \frac{E_{fm}}{x_d} \quad (6)$$

67 Addition of x_T attenuates the magnitude of the currents given in (4), (5) and (6). Secondly, the
 68 rate of dissipation of the stored magnetic energy is increased by the transformer resistance, R_T ,
 69 so that the dc component of short circuit current decays more rapidly. Thirdly, the time constants
 70 are increased by the transformer reactance as given in (7) and (8) [21-23].

$$71 \quad T_{d(network)}'' = T_d'' \left(\frac{X_d'}{X_d''} \right) \left(\frac{X_d'' + X_T}{X_d' + X_T} \right) \quad (7)$$

$$72 \quad T_{d(network)}' = T_d' \left(\frac{X_d}{X_d'} \right) \left(\frac{X_d' + X_T}{X_d + X_T} \right) \quad (8)$$

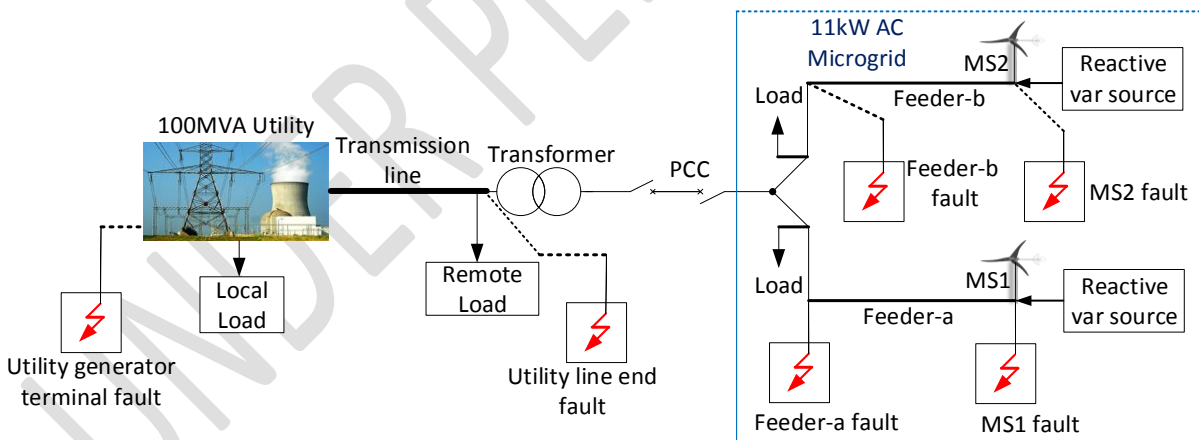
73 **3. Design of control systems**

74 The modeled system is subjected to small signal response analysis. It is found to be stable but its
 75 response time is unsatisfactory. Requisite regulators are then designed using closed-loop
 76 feedback structure. The systems designed are pitch angle regulator, active power management
 77 systems and reactive power management systems. The regulators are combined to implement

78 two mutually exclusive control regimes. These two regimes are active power-voltage (V) control
 79 and reactive-active power (Q) control. Under power-voltage control, the controller maintains
 80 constant grid voltage with a 4% droop. Under reactive-active power control, the controller
 81 ensures constant reactive power at the grid.

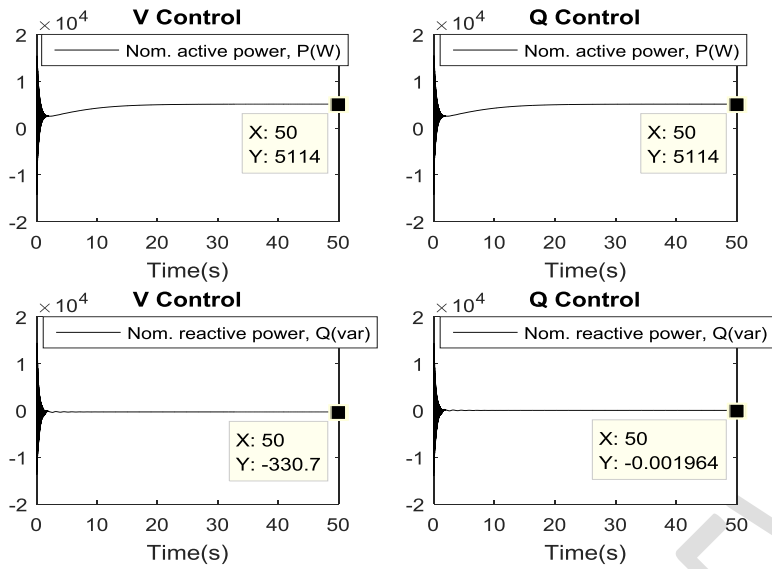
82 4. Short circuit simulation and system dynamic response

83 The testbed developed for this study is shown in fig. 2. In the network, each DFIG is nominally
 84 rated 5.5kW, 575V and linked to 2.5km highly resistive feeder (a or b). Each feeder is connected
 85 to the utility radially at the PCC. A modeled 20MVA STATCOM is connected to the utility side
 86 at the PCC. A local inductive load of 3.6MVA and a remote inductive load of 89.44MVA are
 87 serviced by the utility. A total inductive local load of 6.21kVA is serviced by the microgrid. The
 88 operating frequency of the system is 50Hz, with cut-in and cut-out wind speeds of 3ms^{-1} and
 89 6ms^{-1} , respectively. Islanding of the microgrid is achieved by opening the PCC.



90
 91 **Fig. 2.** A basic diagram displaying the system under study

92 Fig. 3 shows the response of MS1 during normal operation under V and Q controls.



93
94 **Fig. 3.** Response of MS1 under normal operation in V and Q Controls

95 **5. Line-to-line short circuit**

96 Line-to-line short circuit fault is applied at 6.0s and withdrawn at 8.0s. Under this short circuit,
97 system's (microgrid feeders and DFIG) dynamics is simulated for 50.00s. The testbed's
98 responses for different fault locations and DFIG controller in voltage, V, and reactive power, Q,
99 control are obtained and presented in fig. 4 to fig. 19.

100 The responses of MS1 to short circuits at the terminals of utility generator under V and Q
101 controls are presented in fig. 4 and fig. 5, respectively.

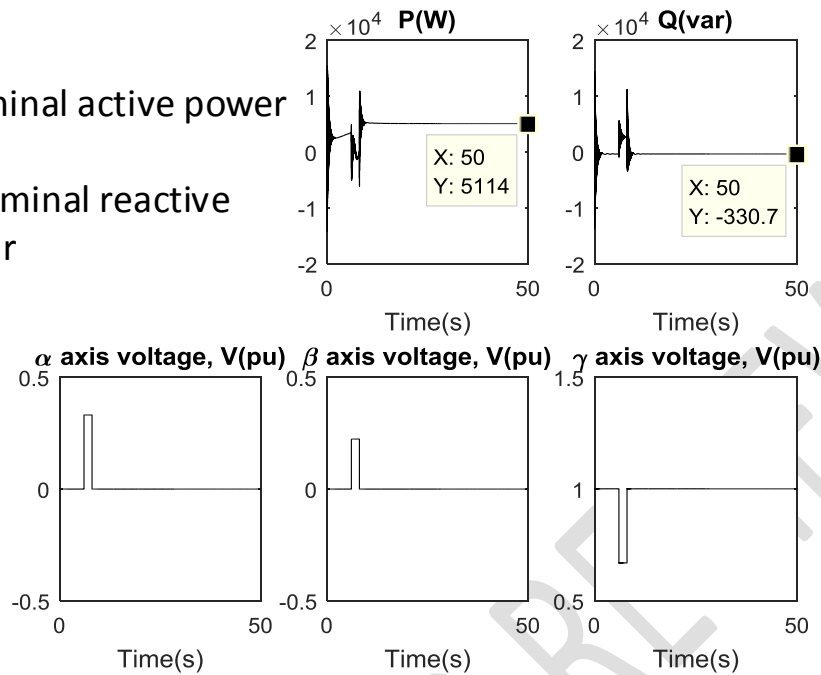
102

103

Key

$P(W)$ = Nominal active power
in Watts

$Q(\text{var})$ = Nominal reactive
power in var



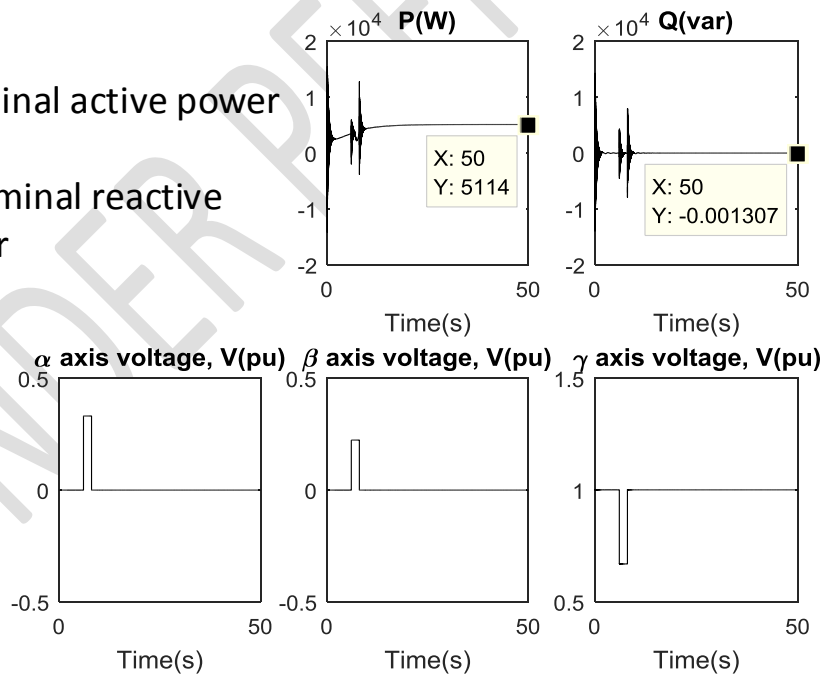
104
105

Fig. 4. Response of MS1 to L-L short circuit – V control

Key

$P(W)$ = Nominal active power
in Watts

$Q(\text{var})$ = Nominal reactive
power in var



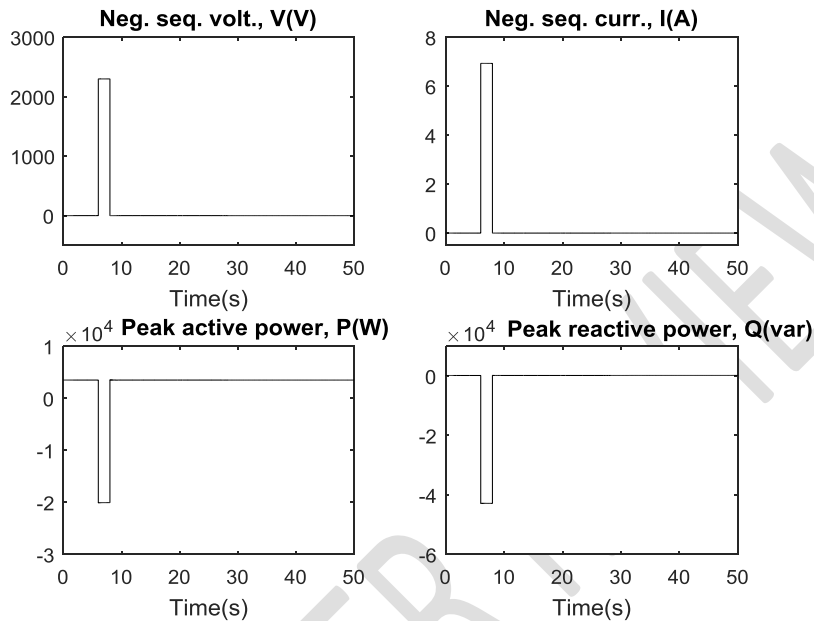
106
107

Fig. 5. Response of MS1 to L-L short circuit – Q control

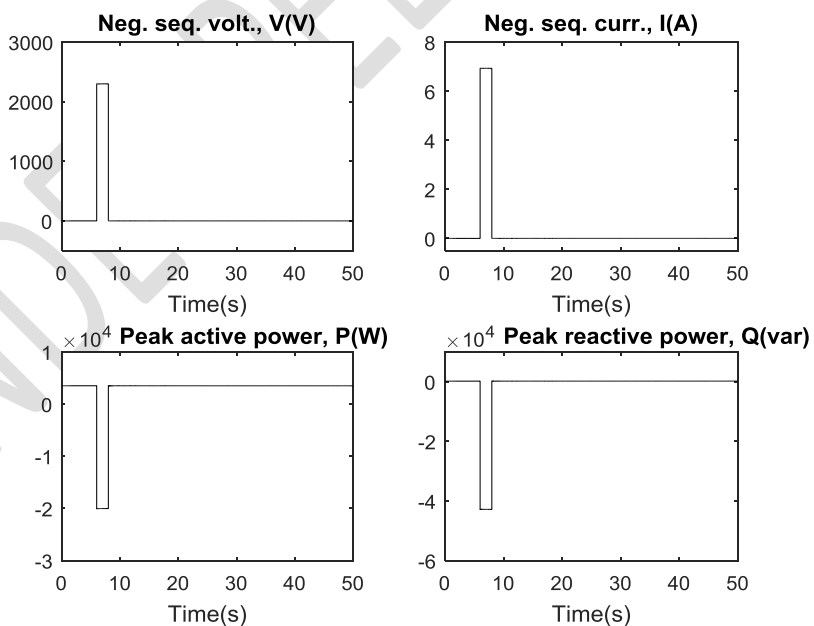
108

109 Fig. 6 shows response of feeder-a to short circuit at terminals of MS1 under V control, while fig.

110 7 shows response of same feeder to same short circuit under Q control.



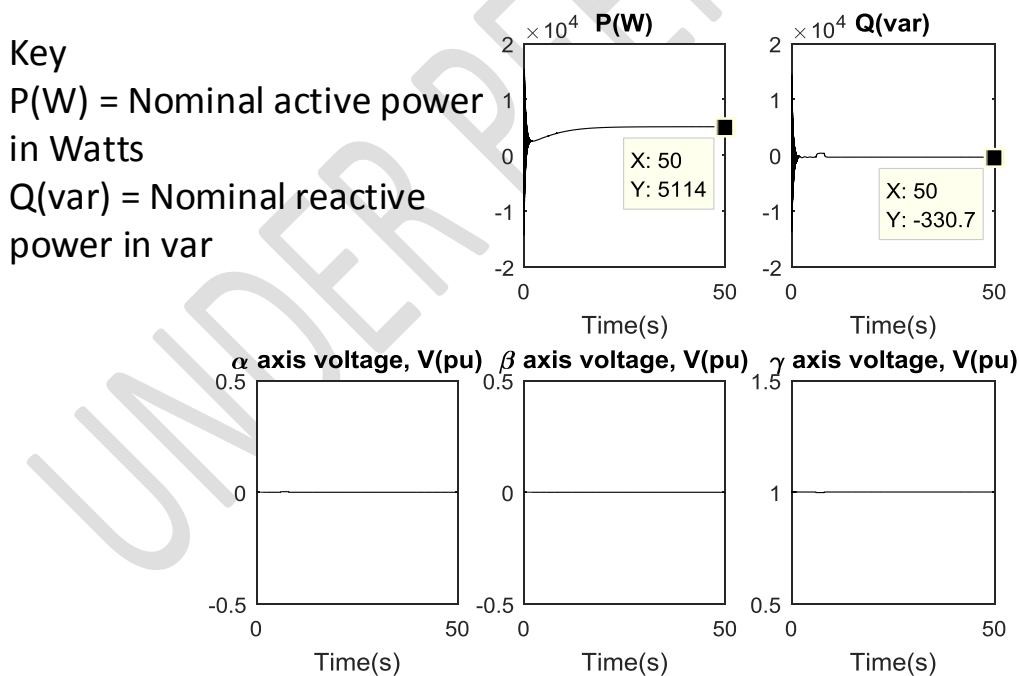
111 **Fig. 6.** Response of feeder-a to L-L short circuit at terminals of MS1– V control



113 **Fig. 7.** Response of feeder-a to L-L short circuit at terminals of MS1– Q control

115

116 Note that under V control (fig. 4) when L-L short circuit is applied at its terminals, MS1 absorbs
 117 330.7var from its reactive var compensator and that of MS2 at 50.00s. This is considerably
 118 higher than 0.001307var it absorbs under Q control (fig. 5), indicative of reactive power
 119 management of DFIG as published by Moayed Moghbel et. al. in [24] and in [25-27]. The peak
 120 active power of feeder-a rose to 20kW in a direction opposite the nominal active power flow
 121 direction during the fault, indicating active power support from MS2 and feeder-b to feed the
 122 fault point in feeder-a. Similarly, reactive power flow on feeder-a rose to more than 40kvar in an
 123 opposite direction during the fault, as seen in fig. 6. Negative sequence quantities only exist
 124 during the fault, as depicted in fig. 6 and fig. 7.
 125 The responses of MS1 to short circuits at the ends of feeder-a under V and Q controls are
 126 presented in fig. 8 and fig. 9, respectively.



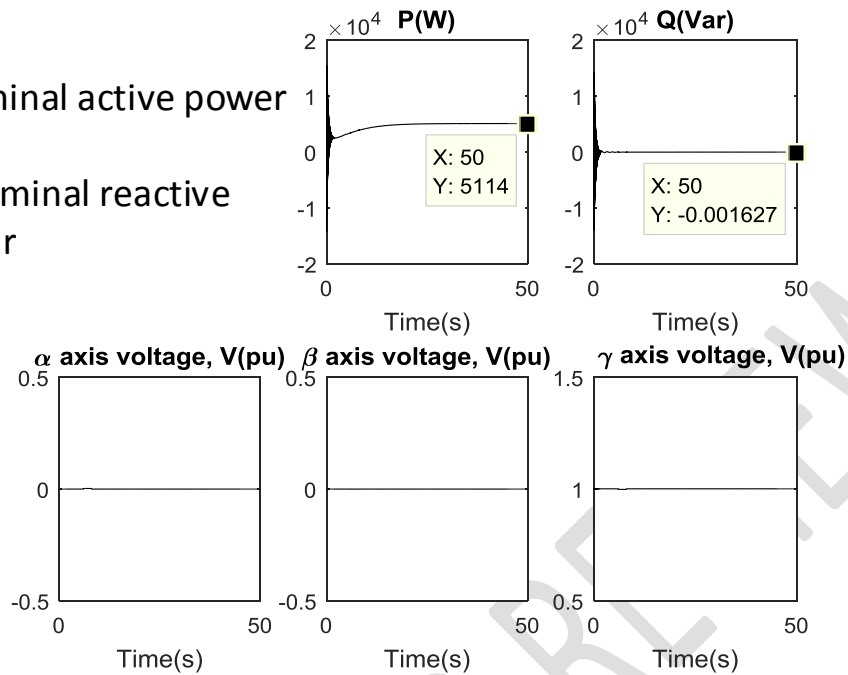
127 **Fig. 8.** Response of MS1 to L-L short circuit at ends of feeder-a – V control
 128

129

Key

$P(W)$ = Nominal active power
in Watts

$Q(\text{var})$ = Nominal reactive
power in var

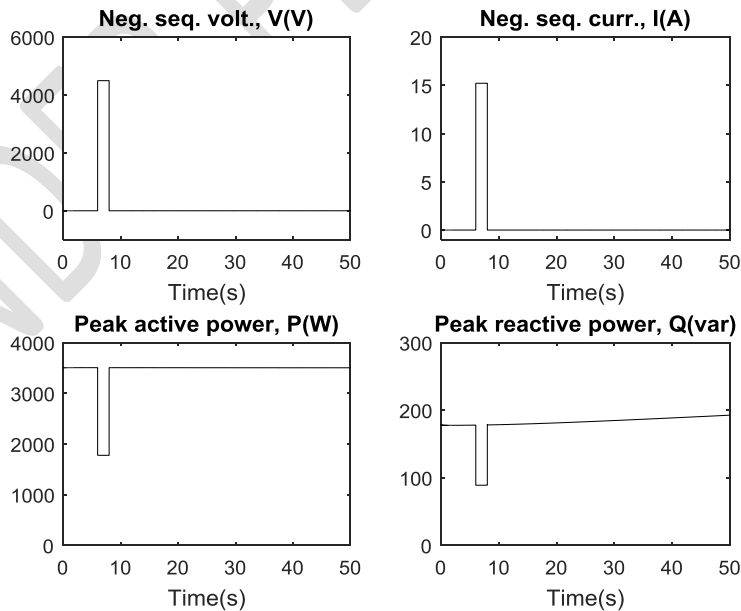


130

131 **Fig. 9.** Response of MS1 to L-L short circuit at ends of feeder-a – Q control

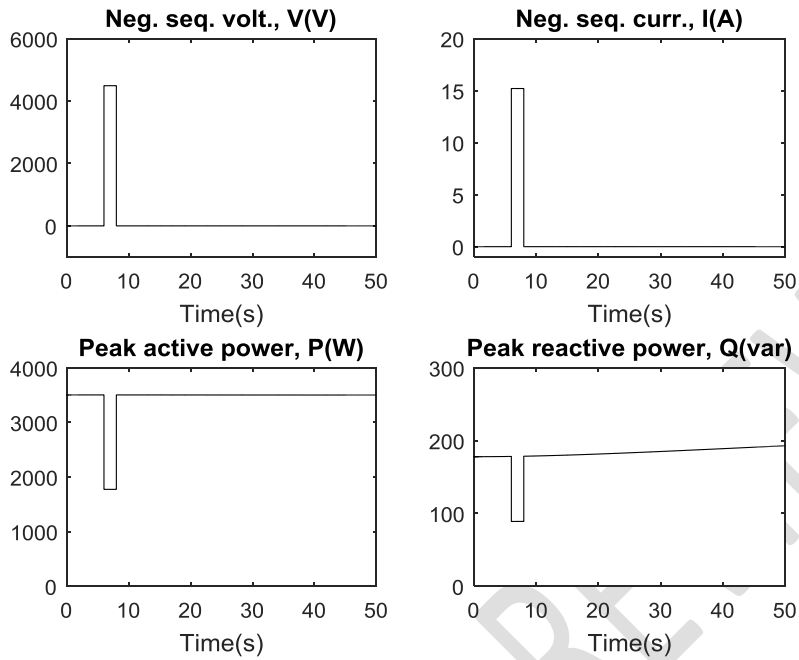
132 Fig. 10 shows response of feeder-a when it is short-circuited under V control, while fig. 11

133 shows response of same feeder to same short circuit under Q control.



134

135 **Fig. 10.** Response of feeder-a when it is short-circuited – V control



136
 137 **Fig. 11.** Response of feeder-a when it is short-circuited – Q control

138

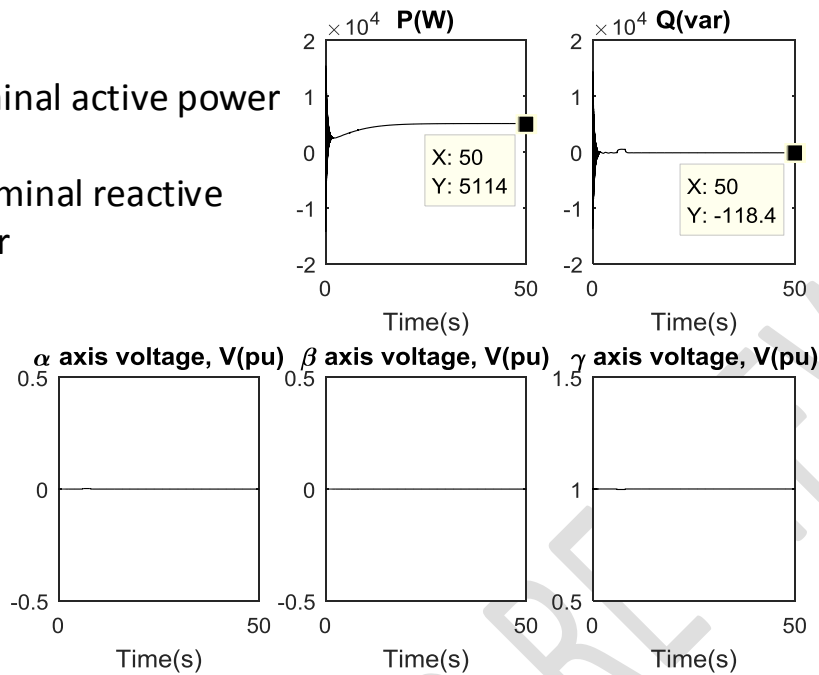
139 Fig. 12 shows response of MS2 when terminals of MS1 are short-circuited under V control,
 140 while fig. 13 shows response of MS2 when terminals of MS1 are short-circuited under Q control.

141

Key

$P(W)$ = Nominal active power
in Watts

$Q(\text{var})$ = Nominal reactive
power in var



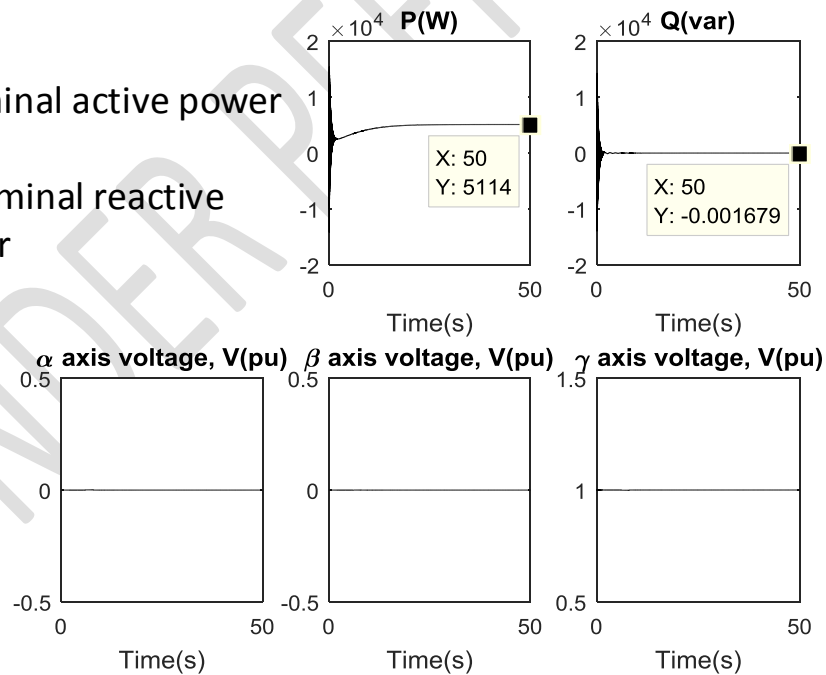
142
143

Fig. 12. Response of MS2 to L-L short circuit at terminals of MS1 – V control

Key

$P(W)$ = Nominal active power
in Watts

$Q(\text{var})$ = Nominal reactive
power in var

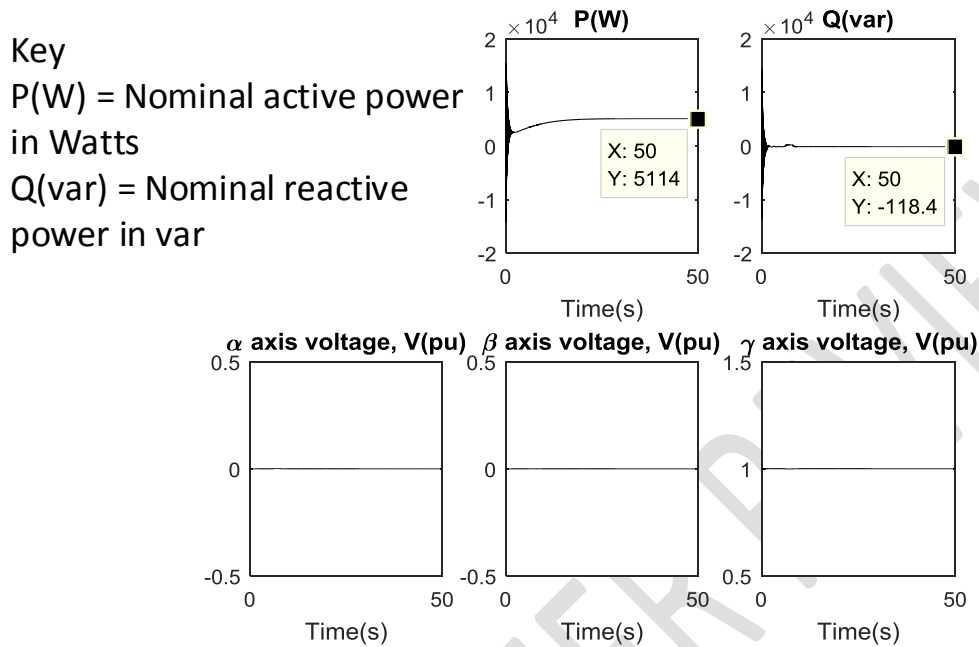


144
145

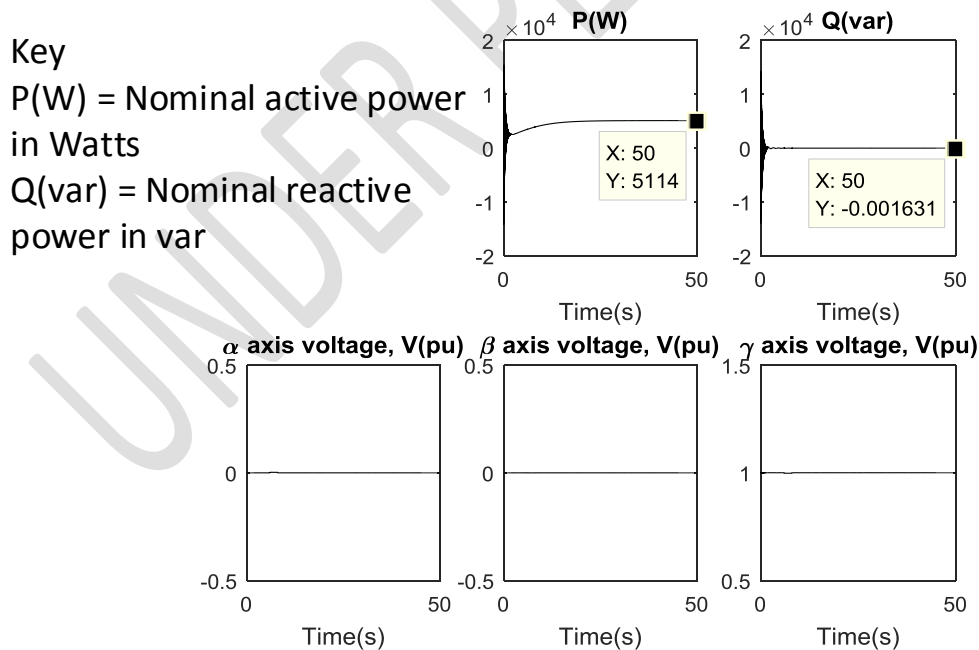
Fig. 13. Response of MS2 to L-L short circuit at terminals of MS1 – Q control

146

147 Fig. 14 shows response of MS2 when ends of feeder-a are short-circuited under V control, while
 148 fig. 15 shows response of MS2 when ends of feeder-a are short-circuited under Q control.



149 **Fig. 14.** Response of MS2 to L-L short circuit at ends of feeder-a – V control
 150



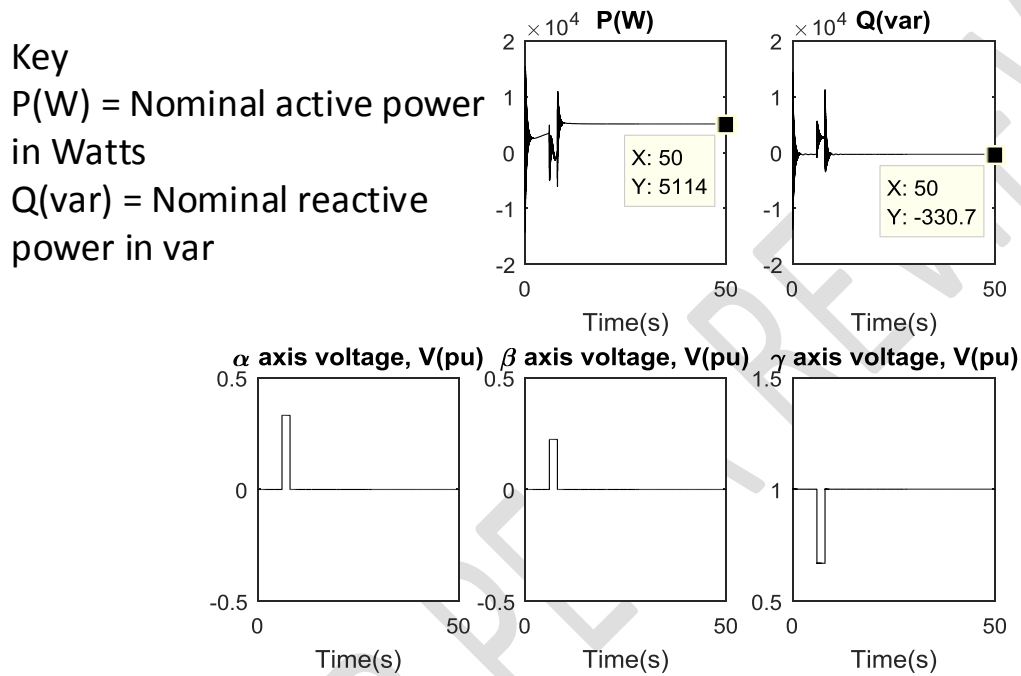
151 **Fig. 15.** Response of MS2 to L-L short circuit at ends of feeder-a – Q control
 152

153

154 Fig. 16 shows response of MS1 to cross-country L-L short circuit at terminals of MS1 and MS2

155 under V control, while fig. 17 shows response of MS1 to same fault as in fig. 16 but under Q

156 control.



157

158 **Fig. 16.** Response of MS1 to cross-country L-L short circuit at terminals of MS1 and MS2 – V

159 control

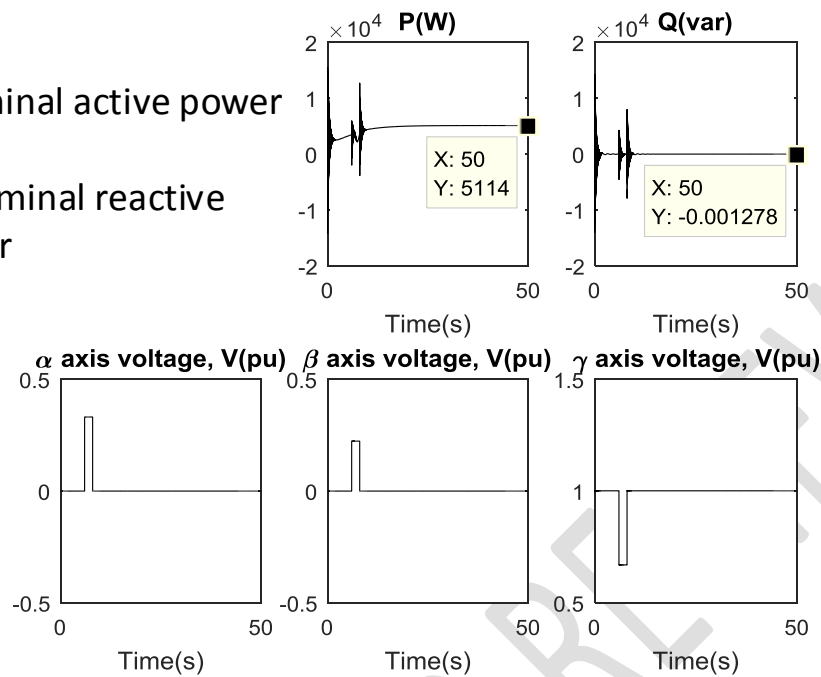
160

161

Key

$P(W)$ = Nominal active power
in Watts

$Q(\text{var})$ = Nominal reactive
power in var



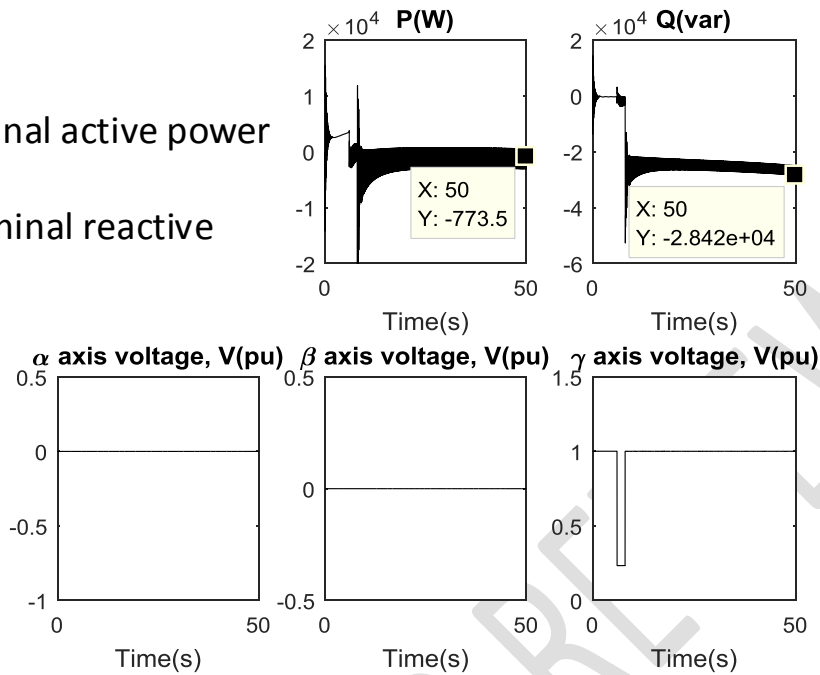
162
163 **Fig. 17.** Response of MS1 to cross-country L-L short circuit at terminals of MS1 and MS2 – Q
164 control

165 6. Three phase bolted short circuit

166 In order to present a peek into the response of the microsource as short circuit severity increases,
167 its response to three phase bolted short circuit is presented in fig. 18 and fig. 19.

168 Fig. 18 and fig. 19 show response of MS1 when three phase-to-ground bolted short circuit is
169 applied at its terminals under V control and Q control, respectively.

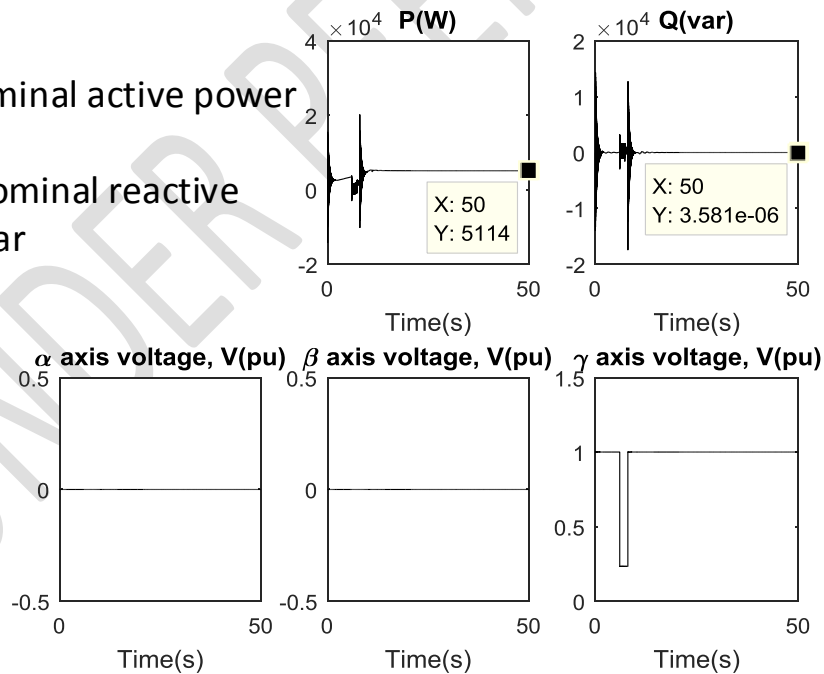
Key
 P(W) = Nominal active power
 in Watts
 Q(var) = Nominal reactive
 power in var



170

171 **Fig. 18.** Response of MS1 to 3-phase bolted short circuit – V control

Key
 P(W) = Nominal active power
 in Watts
 Q(var) = Nominal reactive
 power in var



172

173 **Fig. 19.** Response of MS1 to 3-phase bolted short circuit – Q control

174 **7. Results and discussion**

175 As observed from the simulation results, the generation of each microsource is 92% of its
176 nominal rating when operating under stress-free condition. Similarly, during normal operation,
177 absorption of reactive power of each microsource from the external reactive power compensator
178 is more under V control than Q control. This indicates DFIG's reactive support from its
179 converter dc bus under Q control. This reactive support is, however, unsustainable for continuous
180 operation since the capacitor linked to its converter dc bus is of small capacity.

181 At 50.0s, under V control (fig. 4) when L-L short circuit is applied at its terminals, MS1 absorbs
182 330.7var from its reactive var compensator and that of MS2. This is considerably higher than
183 0.001307var it absorbs under Q control (fig. 5), indicative of reactive power management of
184 DFIG as published by Moayed Moghbel et. al. in [24] and in [25-27]. The peak active power of
185 feeder-a rose to 20kW in a direction opposite the nominal active power flow direction during the
186 fault, indicating active power support from MS2 and feeder-b to feed the fault point in feeder-a.
187 Similarly, reactive power flow on feeder-a rose to more than 40kvar in an opposite direction
188 during the fault, as seen in fig. 5. Negative sequence quantities only exist during the fault, as
189 depicted in fig. 6 and fig. 7.

190 At 50.0s, under V control (fig. 8) when L-L short circuit is applied at ends of feeder-a, MS1
191 absorbs 118.4var from the reactive var compensators. This is considerably higher than
192 0.001627var it absorbs under Q control (fig. 9), indicative of reactive power management of
193 DFIG as published by Moayed Moghbel et. al. in [24] and in [28, 29]. The peak active power of
194 feeder-a dropped to less than 2kW during the fault. Similarly, reactive power flow on feeder-a
195 dropped to less than 100var during the fault, as seen in fig. 10 and fig. 11. Negative sequence
196 quantities only exist during the fault, as depicted in fig. 9 and fig. 11.

197 At 50.0s, under V control (fig. 12) when L-L short circuit is applied at terminals of MS1, MS2
198 absorbs 118.4var from the reactive var compensators. This is considerably higher than
199 0.001679var it absorbs under Q control (fig. 13), indicating reactive power management of DFIG
200 as published by Moayed Moghbel et. al. in [24] and in [28, 29]. The transformed stator voltage
201 of MS2 is undisturbed as the severity of the fault is minimized by the impedance of feeder-a and
202 feeder-b, as shown in fig. 12 to fig. 15.

203 At 50.0s, under V control (fig. 16) when cross-country L-L short circuit is applied at terminals of
204 MS1 and MS2, MS1 absorbs 330.7var from the reactive var compensators. This is considerably
205 higher than 0.001278var it absorbs under Q control (fig. 17), indicating reactive power
206 management of DFIG as published by Moayed Moghbel et. al. in [24] and in [28, 29]. Both
207 active and reactive power of MS1 are unstable during the fault in both V and Q control, but more
208 visible instability is observed under V control regime. Voltage and frequency instability is a
209 major challenge of microgrid operation, as published in [30-32]. During the fault, the
210 transformed stator voltages of MS1 is disrupted in the α , β and γ axes as the severity of the
211 fault is higher than L-L faults that are not cross-country, as shown in fig. 16 and fig. 17.

212 At 50.0s, under V control (fig. 18) when 3-phase bolted short circuit is applied at terminals of
213 MS1, MS1 absorbs (a change of operation from generation mode to motoring mode of DFIG)
214 0.7735kW from MS2 and also absorbs 28.42kvar from the reactive var compensators. This is
215 considerably higher than under Q control regime (fig. 19) where, with same short circuit, MS1
216 generates 5.114kW and supports the system with 3.581×10^{-6} var. This validates reactive power
217 management of DFIG as published by Moayed Moghbel et. al. in [24] and in [28, 29]. Both
218 active and reactive power of MS1 are unstable during the fault in both V and Q control, but

219 virulent and sustained instability is observed under V control regime. Voltage and frequency
220 instability is a major challenge of microgrid operation, as published in [30-32]. The DFIG
221 remained in generation mode under Q control while it changed to motoring mode under V
222 control when exposed to 3-phase bolted short circuit. During the fault, the transformed stator
223 voltages of MS1 is disrupted in the γ axis as the severity of the fault is high, as shown in fig. 18
224 and fig. 19.

225

226 **8. Conclusion**

227 The simulation results of this work has shown that when the system is under 2-second line-to-
228 line short circuit stress, bidirectional flow of active and reactive power between the two feeders
229 occurs, particularly power support at fault points. The simulation has also verified the theory of
230 power management capability of DFIG by showing that each microsource offers superior active
231 and reactive power post-fault stability under Q control than V control when the microgrid is
232 faulted. This is especially obvious as the fault severity increases due to the effect of power
233 electronic (converter and controller) interfacing of DFIG. Finally, the interaction and the
234 engagement of critical quantities in a wind turbine distributed generation with a local load has
235 been explored and depicted. Such is the α, β, γ transformation of DFIG's complex form of stator
236 voltage (a, b, c). Each set of α, β, γ plot shows a unique pattern to fault location, making the
237 α, β, γ transformation a potential candidate for fault sensing and diagnosis – regardless of
238 control regime. In conclusion, the response of the testbed to line-to-line short circuit has been
239 shown to agree with established theory. This helps validate its response to line-to-line short
240 circuit.

241

242

243 **REFERENCES**

- 244 [1] G. Didier, C.H. Bonnard, T. Lubin, J. L  v  que, Comparison between inductive and resistive SFCL in
245 terms of current limitation and power system transient stability, *Electric Power Systems Research*, 125
246 (2015) 150-158.
- 247 [2] D. Filipovi  -Gr  i  , B. Filipovi  -Gr  i  , K. Capuder, Modeling of three-phase autotransformer for
248 short-circuit studies, *International Journal of Electrical Power & Energy Systems*, 56 (2014) 228-234.
- 249 [3] S.V. Papaefthymiou, V.G. Lakiotis, I.D. Margaritis, S.A. Papathanassiou, Dynamic analysis of island
250 systems with wind-pumped-storage hybrid power stations, *Renewable Energy*, 74 (2015) 544-554.
- 251 [4] F. Sulla, J. Svensson, O. Samuelsson, Symmetrical and unsymmetrical short-circuit current of
252 squirrel-cage and doubly-fed induction generators, *Electric Power Systems Research*, 81 (2011) 1610-
253 1618.
- 254 [5] T.-H. Chen, W.-T. Huang, Evaluation of the variations of short-circuit capacities along a feeder due to
255 distribution system-type upgrading, *International Journal of Electrical Power & Energy Systems*, 31
256 (2009) 50-58.
- 257 [6] O.E. Roennspiess, A.E. Efthymiadis, A comparison of static and dynamic short circuit analysis
258 procedures, *IEEE Transactions on Industry Applications*, 26 (1990) 463-475.
- 259 [7] N. Soni, S. Doolla, M.C. Chandorkar, Improvement of Transient Response in Microgrids Using
260 Virtual Inertia, *IEEE Transactions on Power Delivery*, 28 (2013) 1830-1838.
- 261 [8] O. Palizban, K. Kauhaniemi, J.M. Guerrero, Microgrids in active network management – part II:
262 System operation, power quality and protection, *Renewable and Sustainable Energy Reviews*, 36 (2014)
263 440-451.
- 264 [9] I. Patrao, E. Figueres, G. Garcer  , R. Gonz  lez-Medina, Microgrid architectures for low voltage
265 distributed generation, *Renewable and Sustainable Energy Reviews*, 43 (2015) 415-424.
- 266 [10] O.S. Adio, L. Xiangning, Z. Feng, B. Zhiqian, Short circuit analysis for integration of 10MW
267 Windfarm in Nigeria at the PCC, in: 2013 IEEE Power and Energy Society General Meeting (PES),
268 2013, pp. 1-5.
- 269 [11] M. Chaudhary, S.M. Brahma, S.J. Ranade, Short circuit analysis of Type II induction generator and
270 wind farm, in: 2012 IEEE PES Transmission and Distribution Conference and Exposition (T&D) 2012,
271 pp. 1-5.
- 272 [12] A. Mathur, V. Pant, B. Das, Unsymmetrical short-circuit analysis for distribution system considering
273 loads, *International Journal of Electrical Power & Energy Systems*, 70 (2015) 27-38.
- 274 [13] N. Samaan, R. Zavadil, J.C. Smith, J. Conto, Modeling of wind power plants for short circuit
275 analysis in the transmission network, in: Transmission and Distribution Conference and Exposition,
276 2008, T&D;D. IEEE/PES, 2008, pp. 1-7.
- 277 [14] N. Hatziargyriou, H. Asano, R. Iravani, C. Marnay, Microgrids, *IEEE Power and Energy Magazine*,
278 5 (2007) 78-94.
- 279 [15] J.W.B. Jan Machowski, James R. Bumby, *Power System Dynamics and Stability*, John Wiley &
280 Sons, England, 1997.
- 281 [16] R.H. Lasseter, MicroGrids, in: 2002 IEEE Power Engineering Society Winter Meeting, 2002, pp.
282 305-308 vol.301.
- 283 [17] R.J. Best, D.J. Morrow, P.A. Crossley, Current transients in the small salient-pole alternator during
284 sudden short-circuit and synchronisation events, *IET Electric Power Applications*, 4 (2010) 687-700.

- 285 [18] W.H. Kersting, G. Shirek, Short circuit analysis of IEEE test feeders, in: 2012 IEEE PES
286 Transmission and Distribution Conference and Exposition (T&D) 2012, pp. 1-9.
- 287 [19] J. Ouyang, X. Xiong, Research on short-circuit current of doubly fed induction generator under non-
288 deep voltage drop, *Electric Power Systems Research*, 107 (2014) 158-166.
- 289 [20] J. Prajapati, V. Patel, H. Patel, Load flow, short circuit and stability analysis using Matlab, in: *Green*
290 *Computing Communication and Electrical Engineering (ICGCCEE)*, 2014 International Conference on,
291 2014, pp. 1-5.
- 292 [21] A. Bracale, P. Caramia, A.R. Di Fazio, D. Proto, Probabilistic short circuit analysis in electric power
293 distribution systems including distributed generation, in: *8th Mediterranean Conference on Power*
294 *Generation, Transmission, Distribution and Energy Conversion (MEDPOWER 2012)*, 2012, pp. 1-6.
- 295 [22] T. Jen-Hao, Unsymmetrical Short-Circuit Fault Analysis for Weakly Meshed Distribution Systems,
296 *IEEE Transactions on Power Systems*, 25 (2010) 96-105.
- 297 [23] J. Ouyang, X. Xiong, Dynamic behavior of the excitation circuit of a doubly-fed induction generator
298 under a symmetrical voltage drop, *Renewable Energy*, 71 (2014) 629-638.
- 299 [24] M. Moghbel, H.T. Mokui, M.A.S. Masoum, M. Mohseni, Reactive power control of DFIG wind
300 power system connected to IEEE 14 bus distribution network, in: *Universities Power Engineering*
301 *Conference (AUPEC)*, 2012 22nd Australasian, 2012, pp. 1-7.
- 302 [25] X. Dongliang, X. Zhao, Y. Lihui, J. Ostergaard, X. Yusheng, W. Kit Po, A Comprehensive LVRT
303 Control Strategy for DFIG Wind Turbines With Enhanced Reactive Power Support, *IEEE Transactions*
304 *on Power Systems*, 28 (2013) 3302-3310.
- 305 [26] J. Jeong-Ik, K. Young-Sin, L. Dong-Choon, Active and Reactive Power Control of DFIG for Wind
306 Energy Conversion under Unbalanced Grid Voltage, in: *IEEE 5th International Power Electronics and*
307 *Motion Control Conference 2006, IPERC 2006*, 2006, pp. 1-5.
- 308 [27] M. Kayikci, J.V. Milanovic, Reactive Power Control Strategies for DFIG-Based Plants, *IEEE*
309 *Transactions on Energy Conversion*, 22 (2007) 389-396.
- 310 [28] S.A. Gopalan, V. Sreeram, H.H.C. Iu, A review of coordination strategies and protection schemes for
311 microgrids, *Renewable and Sustainable Energy Reviews*, 32 (2014) 222-228.
- 312 [29] E. Planas, A. Gil-de-Muro, J. Andreu, I. Kortabarria, I. Martínez de Alegría, General aspects,
313 hierarchical controls and droop methods in microgrids: A review, *Renewable and Sustainable Energy*
314 *Reviews*, 17 (2013) 147-159.
- 315 [30] R. Romo, O. Micheloud, Power quality of actual grids with plug-in electric vehicles in presence of
316 renewables and micro-grids, *Renewable and Sustainable Energy Reviews*, 46 (2015) 189-200.
- 317 [31] M. Soshinskaya, W.H.J. Crijns-Graus, J.M. Guerrero, J.C. Vasquez, Microgrids: Experiences,
318 barriers and success factors, *Renewable and Sustainable Energy Reviews*, 40 (2014) 659-672.
- 319 [32] R. Zamora, A.K. Srivastava, Controls for microgrids with storage: Review, challenges, and research
320 needs, *Renewable and Sustainable Energy Reviews*, 14 (2010) 2009-2018.

321